J. Phys. B: At. Mol. Opt. Phys. 24 (1991) 1087–1106. Printed in the UK

Theoretical study of low-energy electron–SiH_4 collisions using exact-exchange plus parameter-free polarization potential

Ashok Jain† and D G Thompson‡

† Department of Physics, Florida A & M University, Tallahassee, Florida 32307, USA
‡ Department of Applied Mathematics and Theoretical Physics, The Queen's University, Belfast, BT7 1NN, UK

Received 7 August 1990, in final form 9 November 1990

Abstract. We investigate rotationally elastic, inelastic and summed processes in the e–SiH_4 collisions at 0.001–20 eV. In these calculations, the electron exchange interaction is treated exactly in an iterative approach, while the target charge correlation and polarization effects are included using a parameter-free model polarization potential based on the second-order perturbation energy. The coupled integro-differential equations are set up in the one-centre-expansion scheme under the fixed-nuclei approximation. Results on the differential, integral, momentum transfer, viscosity and energy-loss cross sections are presented and compared with other available data (both theoretical and experimental). The value of the scattering length is also reported.

1. Introduction

This paper is an extension of our recent work on the electron (e)–CH_4 low-energy ($E \leq 20$ eV) collisions (McNaughten and Thompson 1988, Jain *et al* 1989, McNaughten *et al* 1990) to another similar but heavier spherical top silane (SiH_4) molecule. In these calculations for the e–CH_4 system, we demonstrated for the first time, deficiencies of the popular free-electron-gas–exchange (FEGE) model (Hara 1967, Salvini and Thompson 1981) for electron exchange effects in the low-energy region. The nonlocal exchange interaction of the e–CH_4 system was treated properly by solving the corresponding coupled integro-differential equations iteratively (see, McNaughten and Thompson 1988). It was found that the differential (DCS), total (σ_t) and momentum transfer (σ_m) cross sections in the Ramsauer–Townsend (RT) minimum and shape resonance regions are very sensitive to the exact treatment of the exchange term. In addition, the rotationally inelastic processes were also found to be quite sensitive to the approximations involved in the treatment of exchange and polarization forces (McNaughten *et al* 1990).

The present work on e–SiH_4 scattering is essential from several points of view: first, recently, absolute measurements have been carried out for both the total (Wan *et al* 1989) and differential (Tanaka *et al* 1990) cross sections at low energies and, to the best of our knowledge, no calculation, treating exchange effects exactly along with a model but parameter-free polarization potential, is available on the low-energy scattering parameters for the e–SiH_4 system; second, it is interesting and essential to test

0953-4075/91/051087+20$03.50

our earlier ESEP (exact-static-exchange plus the polarization potential) model (McNaughten and Thompson 1988, McNaughten *et al* 1990) for a molecular system which is heavier and more polarizable than the CH_4 molecule; third, the e–SiH_4 collision process exhibits the RT effect below 1 eV (see Kurachi and Nakamura 1989, Hayashi 1987, Mathieson *et al* 1987, Ohmori *et al* 1986, Garscadden *et al* 1983, Pollock 1968) and is also characterized by a shape resonance phenomenon around 2–3 eV (Wan *et al* 1989, Tronc *et al* 1989, Tossell and Davenport 1985, Sueoka and Mori 1985, Giordan 1983); fourth, a large discrepancy exists between all previous calculations (Yuan 1989, Jain and Thompson 1987, Jain *et al* 1987, Jain 1987, Gianturco *et al* 1987, Tossell and Davenport 1984) and the experimental cross sections for low-energy e–SiH_4 total cross sections; finally, the e–SiH_4 scattering cross section data are needed in many applied sciences (see, for example, Garscadden *et al* 1983).

Here, we are concerned mainly with the exact treatment of the exchange interaction in the e–SiH_4 collision. The only published results on the e–SiH_4 system treating exchange exactly (plus an approximate polarization potential) are due to Yuan (1989). The calculations of Yuan (1989) are, however, done using a spherical approximation for the target wavefunction, projectile function and the interaction potential of the e–SiH_4 system. Therefore, these cross sections (Yuan 1989) may not be accurate, for example, at low energies, for the DCS parameter and at those energies where the rotational channel is important. More recently, Winstead *et al* (1990) have reported their preliminary results on the e–SiH_4 system at the exact-static-exchange (ESE) (without including polarization effects) level by using Schwinger multichannel theory; however, these calculations may not be suitable for comparison with measured values due to neglect of charge correlation and polarization effects.

In the next section 2, we describe briefly the theoretical model, formulae for cross sections and the numerical part of the calculations. In section 3, we present our results for various differential and integral quantities, while, finally in section 4, we make some concluding remarks.

2. A review of theoretical approach

2.1. Exact exchange plus the polarization model

At the static-exchange level (see, Gianturco and Jain 1986), the Schrödinger equation for the continuum electron function $F(\boldsymbol{r})$ in the body-fixed (BF) coordinate system can be written as,

$$\left(-\tfrac{1}{2}\nabla^2 + V_s(\boldsymbol{r}) - \tfrac{1}{2}k^2\right)F(\boldsymbol{r}) = \sum_\alpha \int \phi_\alpha^*(\boldsymbol{r}')|\boldsymbol{r}-\boldsymbol{r}'|^{-1}F(\boldsymbol{r}')\,\mathrm{d}\boldsymbol{r}'\,\phi_\alpha(\boldsymbol{r}) \tag{1}$$

where k is the incident electron wavevector and the static potential V_s is given by

$$V_s(\boldsymbol{r}) = \int |\Phi_0|^2 \left(\sum_{j=1}^{N} |\boldsymbol{r}-\boldsymbol{r}_j|^{-1}\,\mathrm{d}\boldsymbol{r}_1\,\mathrm{d}\boldsymbol{r}_2 \ldots \mathrm{d}\boldsymbol{r}_N\right) - \sum_{i=1}^{M} Z_i|\boldsymbol{r}-\boldsymbol{R}_i|^{-1}. \tag{2}$$

Here Φ_0 is the target ground state wavefunction given as a single Slater determinant of one-electron N spin orbitals $\phi_i(\boldsymbol{r})$ and M is the number of nuclei in the molecule.

In the static-exchange approximation (1), not all the short-range correlation is included and long-range polarization of the target charge cloud is totally neglected. However, these effects (particularly the long-range polarization) must be included for a proper description of low-energy electron scattering and also for a comparison with experimental data. In the present work, we have allowed for charge distortion effects approximately by introducing a local and real polarization potential $V_{\text{pol}}(r)$ in (1). In brief, the V_{pol} is parameter-free and calculated by the method of Pople and Schofield (1957) (PS) and the non-penetration criterion of Temkin (1957). In the PS method (see Jain and Thompson 1982, 1983, Jain 1983), the second-order energy of the target is determined from the first-order target wavefunction Φ_1 which is expanded in terms of Φ_0 and the expansion coefficients are evaluated variationally. The polarizibility (α_0) of the SiH_4 molecule determined from the PS method is 43.4 au, which is about 43% higher than the experimental value of 30.4 au (Hill *et al* 1969). This large difference is expected to be due to limitations of the PS method and of the Hartree–Fock basis set for such a heavy system with 18 electrons. We thus normalize the PS polarization potential to yield the correct asymptotic behaviour of V_{pol} (to be denoted in the following as the JT polarization potential).

Finally, after projecting the inhomogeneous equation (1) onto the symmetry-adapted angular basis functions of $F(r)$, we obtain a set of coupled integro-differential equations which can be written in a convenient matrix form, $\mathbf{LF} = \mathbf{WF}$, where $\mathbf{WF}$ is the exchange term. The iterative scheme is $\mathbf{LF}^i = \mathbf{WF}^{i-1}$, where $i = 0, 1, \ldots$. In order to start the solution, we chose $\mathbf{F}^0$ to be the solutions obtained from the FEGE potential (Jain and Thompson 1987). The equation (1) is solved for each symmetry (A_1, E, T_1 and T_2; we do not include the A_2 symmetry due to its small contribution to scattering parameters) and energy separately. The convergence of the reaction matrix with respect to number of iterations was tested for each state and also at the lower and the upper ends of the present energy region. We faced no convergence problems with or without polarization effects. For the present SiH_4 case, the other convergence parameters (the size of $\mathbf{K}$ matrix, expansion of potential terms and number of terms in the expansion of bound orbitals) were checked carefully and these details are exactly the same as described earlier (Jain and Thompson 1987).

2.2. Cross section formulae

For full details, we refer to a recent review by Gianturco and Jain (1986). Here, we provide only a summary of various cross section quantities. As mentioned earlier, we study here only rotationally elastic, inelastic and summed channels for differential, integral, momentum-transfer and energy-loss cross sections. In order to obtain collisional parameters, we transform the BF scattering amplitude $f(\hat{\boldsymbol{k}} \cdot \hat{\boldsymbol{r}})$ ($\hat{\boldsymbol{k}}$ and $\hat{\boldsymbol{r}}$ are respectively the initial and final directions of the projectile) into space-fixed (SF) amplitude $f(\hat{\boldsymbol{k}} \cdot \hat{\boldsymbol{r}}'; \alpha\beta\gamma)$ (where $\hat{\boldsymbol{r}}'$ now refers the direction of scattered electron with respect to SF coordinate system and $(\alpha\beta\gamma)$ are the three Euler angles) by making use of rotation matrices. Even at the lower bound of the present energy region, the collision time is much less than the molecular rotational time period; hence, the adiabatic-nuclei-rotation (ANR) approximation is valid and the scattering amplitude for a particular rotational transition $JKM \rightarrow J'K'M'$ can be written as (Chase 1956)

$$f(JKM \rightarrow J'K'M') = \langle \psi_{JKM} | f(\hat{\boldsymbol{k}} \cdot \hat{\boldsymbol{r}}'; \alpha\beta\gamma) | \psi_{J'K'M'} \rangle \tag{3}$$

where the $|\psi_{JKM}\rangle$ represents the rotational eigenfunctions of a spherical top defined

as

$$\psi_{JKM}(\alpha\beta\gamma) = \left(\frac{2J+1}{8\pi^2}\right)^{1/2} D^{J*}_{KM}(\alpha\beta\gamma). \tag{4}$$

Here K and M are the projections of J along the BF and SF frame principal axes respectively. The DCS for a particular $J \rightarrow J'$ transition is obtained by summing over all final magnetic substates $K'M'$ and averaging over all initial substates KM, i.e.,

$$\frac{\mathrm{d}\sigma}{\mathrm{d}\Omega}(J \rightarrow J') = \frac{k'}{k}\frac{1}{(2J+1)^2}\sum_{MM'KK'} |f(JKM \rightarrow J'K'M')|^2 \tag{5}$$

where the final wavevector k' is calculated from the following relation

$$2k'^2 = 2k^2 + E_J - E_{J'}. \tag{6}$$

The energy of the Jth rotational level is given by $E_J = BJ(J+1)$, where B is the rotational constant of SiH_4 molecule. The value of B is taken to be 3.55×10^{-4} eV. It is convenient to expand the DCS in terms of Legendre polynomials,

$$\frac{\mathrm{d}\sigma}{\mathrm{d}\Omega}(J \rightarrow J') = \frac{k'}{k}\sum_L A_L(J \rightarrow J')P_L(\cos\theta). \tag{7}$$

Here θ is the scattering angle between the vectors $\hat{\boldsymbol{k}}$ and $\hat{\boldsymbol{r}}'$. The expansion A_L coefficients are given as (Jain 1983)

$$\begin{aligned} A_L(J \rightarrow J') = {} & \frac{(2J'+1)(2L+1)(-1)^L}{4k^2(2J+1)} \\ & \times \sum_{ll'\bar{l}\bar{l}'}[(2l+1)(2l'+1)(2\bar{l}+1)(2\bar{l}'+1)]^{1/2} \mathrm{i}^{l-l'}(-\mathrm{i})^{\bar{l}-\bar{l}'} \\ & \times \begin{pmatrix} \bar{l} & l & L \\ 0 & 0 & 0 \end{pmatrix}\begin{pmatrix} l' & \bar{l}' & L \\ 0 & 0 & 0 \end{pmatrix} \sum_{j=|J-J'|}^{J+J'} (-1)^j W(ll'\bar{l}\bar{l}'; jL) M^{jm_j}_{ll'} M^{jm_j *}_{\bar{l}\bar{l}'} \end{aligned} \tag{8}$$

where the M matrix is constructed as

$$M^{jm_j}_{ll'} = \sum_{mm'hh'p\mu} (-1)^m \bar{b}^{p\mu}_{lhm}\begin{pmatrix} l & l' & j \\ m & m' & -m_j \end{pmatrix}\bar{b}^{p\mu}_{l'h'm'}\, \mathbf{T}^{p\mu}_{lh,l'h'}. \tag{9}$$

Here, as usual, the $\mathbf{T}$ matrix is defined in terms of the $\mathbf{S}$ matrix as $\mathbf{T} = (\mathbf{S} - 1)$ where $\mathbf{S} = (1 + \mathrm{i}\mathbf{K})(1 - \mathrm{i}\mathbf{K})^{-1}$ is written in terms of scattering $\mathbf{K}$ matrix for each symmetry $(p\mu)$. In (8), $\begin{pmatrix} a & b & c \\ d & e & f \end{pmatrix}$ is a 3-j symbol, $W(abcd;ef)$ is the Racah coefficient and the $b^{p\mu}_{lhm}$ coefficients are expansion terms in the definition of symmetry-adapted basis functions in terms of real spherical harmonics (see Gianturco and Jain 1986). From equation (6), it is easy to derive simple forms for the σ_t and σ_m cross sections in terms of A_L coefficients, namely

$$\sigma_t^{JJ'} = 4\pi A_0(J \rightarrow J') \qquad \sigma_m^{JJ'} = 4\pi[A_0(J \rightarrow J') - \tfrac{1}{3}A_1(J \rightarrow J')]. \tag{10}$$

It is straightforward to determine A_0 and A_1 coefficients for σ_t and σ_m rather than the full expansion (7), (8) for the DCS. For example, the A_0 and A_1 are given by the following simpler expressions,

$$A_0 = \frac{1}{4k^2} g(JJ') \sum_{ll'jm_j} (-1)^{l+l'} |M_{ll'}^{jm_j}|^2 \tag{11}$$

and

$$\begin{aligned} A_1 = \frac{3}{4k^2} g(JJ') \sum_{ll'jm_j} (-1)^{l+l'+j} [\{(l+1)(l'+1)\}^{1/2} W(ll'l+1l'+1;j1) M_{ll'}^{jm_j} M_{l+1l'+1}^{jm_j^*} \\ + \{l(l'+1)\}^{1/2} W(ll'l-1l'+1;j1) M_{ll'}^{jm_j} M_{l-1l'+1}^{jm_j^*} \\ + \{(l+1)l'\}^{1/2} W(ll'l+1l'-1;j1) M_{ll'}^{jm_j} M_{l+1l'-1}^{jm_j^*} \\ + (ll')^{1/2} W(ll'l-1l'-1;j1) M_{ll'}^{jm_j} M_{l-1l'-1}^{jm_j^*}] \end{aligned} \tag{12}$$

where $g(JJ')$ represents the statistical $(2J'+1)/(2J+1)$ factor. The vibrationally elastic (rotationally summed) cross sections are obtained by summing over J' for $J = 0$. The selection rule for the transition $J \rightarrow J'$ can easily be worked out from the asymptotic form of the static potential (2) which transforms as $^1A_1$ symmetry of the T_d point group. For any specified values of J and J', the angular momentum transfer j (equations (8) and (9)) takes the following values

$$|J - J'| \leq j \leq J + J' \qquad |l - l'| \leq j \leq l + l'. \tag{13}$$

The selection rules for the rotational transitions are discussed earlier (Jain and Thompson 1983). For example, for $J = 0$, the allowed values of J' are $0, 3, 4, \ldots$, i.e. $|J - J'| = 0, 3, 4, 6, \ldots$ and so on. The rotational energy-loss differential cross section for a particular initial state J is given by (Norcross 1982)

$$\frac{dS^J}{d\Omega} = \sum_{J'} \frac{1}{2}(k^2 - k'^2) \frac{d\sigma}{d\Omega}(J \rightarrow J'). \tag{14}$$

The corresponding integral of (14) over scattering angles will be represented by S^J, known as the stopping cross section corresponding to initial rotational state J. We will show our results for S^0 and S^1 and discuss a general theorem by Shimamura (1981, 1983) which states that the energy-loss and stopping (as well as DCS and σ_t) cross sections are, when summed over final rotational states, independent of the initial rotational state of the molecule in a situation where the rotational motion of the molecule is small during the collision time. Finally the viscosity cross section (σ_v) can be evaluated easily from the DCS by integrating them with a weighting factor of $\sin^2\theta$.

2.3. Numerical details

As mentioned earlier, our earlier paper (Jain and Thompson 1987) gives most of the information about the e–SiH_4 bound and scattering functions. The single-centre symmetry-adapted wavefunctions for the $^1A_1$ ground electronic state of SiH_4 were

generated using an unpublished code of F A Gianturco and U Lamana. The single-centre expansion of bound orbitals included terms up to $l = 6$; thus, 10 terms for the a_1, 13 for the t_{2z} and 17 each for the t_{2x} and t_{2y} type bound orbitals. This basis set gave a value 3.67×10^{-34} esu for the octupole moment as compared to the experimental value of 2.4 (Birnbaum and Cohen 1976) in the same units. The single-centre expansion of the static potential is truncated at $\lambda = 6$, i.e.

$$V_s(r) = \sum_{\lambda=0}^{6} \sum_{m} v_{\lambda m}(r) S_\lambda^{mA_1}(\hat{r}). \tag{15}$$

Due to the tetrahedral symmetry of silane, there are only four terms in (15). The details and numerical values of the polarization potential are exactly the same as given in Jain and Thompson (1987). The size of the **K** matrix with $l = 6$ for A_1, E (E_x and E_y), T_1 and T_2 scattering states is 4, 4, 4 and 5 respectively. We kept the *maximum* l value fixed at each energy considered in this paper The radial mesh of all bound, continuum and potential terms was very fine (0.001 au). The maximum value of r was taken to be 18.8 au before using the asymptotic solutions. The symmetric nature and the convergence of the final **K** matrices were checked carefully for each irreducible representation and each energy with respect to the number of iterations. At lower energies, we needed as many as 30 iterations for proper convergence; however, above 1 eV, about 15 iterations were enough to obtain converged **K** matrices for each symmetry.

3. Results and discussion

3.1. Elastic (rotationally summed) cross sections

Let us first discuss the qualitative features of low-energy e–SiH_4 cross sections such as the Ramsauer–Townsend minimum below 1 eV and a 3–4 eV shape resonance phenomenon. Figures 1–2 illustrate the eigenphase sums for various scattering symmetries in the 0.1–20 eV region. It is clear from figure 1 that the present ESEP (full curve) is responsible for (nearly) the correct position of the minimum (around 0.25 eV in a recent swarm study of Kurachi and Nakamura 1989) due to the A_1 scattering symmetry. Note that our earlier SMEP (static, FEGE and the JT polarization potentials) results (Jain and Thompson 1987) or the present ESE (without polarization) curves are incorrect in this low-energy region. The value of the position of this minimum as obtained by Yuan (1989) in the spherical approximation is quite low (around 0.11 eV). Other calculations, where exchange is treated via a model local potential (Gianturco *et al* 1987, Jain *et al* 1987), do not give reliable results in this rather low-energy region. In figure 2, we have shown the eigenphase sums for the T_2 and E symmetries above 1 eV. Also shown in this figure is the SMEP curve for the T_2 state. The ESEP curve clearly exhibits a shape resonance phenomenon around 3.75 eV; this structure is due to the d-wave of the incoming electron's partial waves. Therefore, the E symmetry (which also have a d-wave component) also exhibits a weak shape resonance feature at about 4 eV. As we will see later, the ESEP curve is more realistic than our previous model exchange (FEGE) calculation (the broken curve of figure 2 is due to Jain and Thompson 1987).

It may be interesting to see the corresponding behaviour of the ESEP partial cross sections in various scattering states. This is illustrated in figure 3 for all the dominating

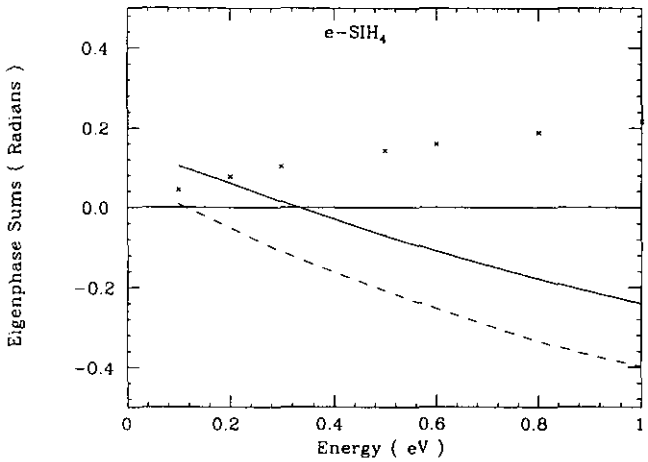

Figure 1. Eigenphase sums for the e–SiH_4 collisions in A_1 symmetry in the present ESEP (full curve) and ESE (crosses) models. The broken curve is the SMEP calculation of Jain and Thompson (1987). For various notations, see the text.

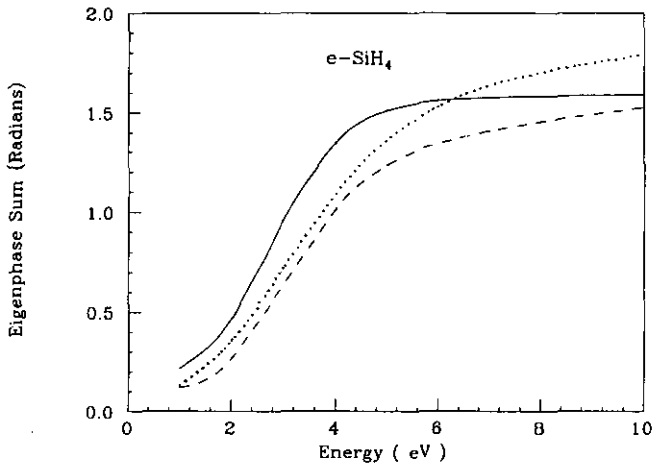

Figure 2. Eigenphase sums for the e–SiH_4 collision in the T_2 (full curve) and E (dotted curve) symmetries by using the present ESEP model. The broken curve represents the SMEP values of Jain and Thompson (1987) for the T_2 state.

states (A_1, E and T_2) below (curve 3(a)) and above (curve 3(b)) 1 eV impact energy. Here we see a visual effect of the minimum and the maximum in the cross sections for various scattering states. In these figures (3(a) and 3(b)), we have also included SMEP results of Jain and Thompson (1987) for the A_1 and T_2 states for comparison.

We now discuss our rotationally summed (vibrationally and electronically elastic) differential cross sections in the energy range from 1.8 to 20 eV, where recent absolute measured values are available (Tanaka *et al* 1990). These results are depicted in figures 4(a)–(j) alongwith the experimental data of Tanaka *et al* (1990). For comparison, we also show our ESE results (broken curves in figures 4(a)–(j)) where polarization effects are switched off. This comparison (between full and broken curves) gives us an idea

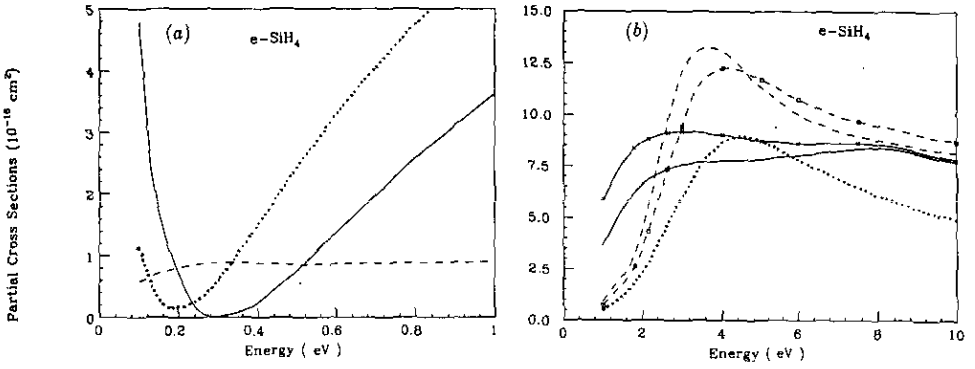

Figure 3. (*a*) Partial cross sections at 0–1 eV energy range for the e–SiH_4 system in A_1 (full curve) and T_2 (broken curve) scattering states. The dotted curve represents the SMEP calculations of Jain and Thompson (1987) for the A_1 representation. (*b*) As (*a*) but in the 1–20 eV region. The full and broken curves marked with crosses (A_1 state) and squares (T_2 state) are the corresponding results of Jain and Thompson (1987). The dotted curve is our ESEP calculation for the E symmetry.

about the importance of polarization effects in this energy range for various angular regions. We can clearly see that the polarization interaction changes the shape (and magnitude too) of the DCS at all energies considered here (cf figures 4(*a*)–(*j*)), but particularly at energies 4–10 eV (figures 4(*d*)–(*h*)). Experiment cannot distinguish between the two calculations except at 7.5 eV and 10 eV (figures 4(*g*) and (*h*)) where agreement is better with the ESEP approximation.

We also notice that the polarization effects are more important in the resonance region (see the DCS at 3, 4 and 5 eV in figures 4(*d*), 4(*e*) and 4(*f*) respectively), where the structure in the DCS reflects the d-wave dominance. This is expected since polarization interaction influences the shape resonance region considerably. In general, the agreement with experimental data is reasonable. The dip at about 55° observed at 1.8 and 2.15 eV by Tanaka *et al* (1990) is shifted in our results towards lower angle by about 10°. The second dip occurring in our DCS around 130° at 1.8 and 2.15 eV, seems to be shifted in the same fashion as the lower angle dip with respect to the experimental data (however, the measured values are not available above 130° angle).

At somewhat higher energies ($E \gtrsim 3$ eV), the two dips in the DCS are still visible, while such a structure in the measured angular functions is quite weak. It may be interesting to compare our DCS with another set of absolute experimental data (not available right now). The present predicted DCS values may be quite useful for normalizing purposes in future measurements. No other theoretical calculations are available for the DCS of e–SiH_4 collisions in this energy range. Therefore, we provide our ESEP DCS values in tabular form in tables 1 and 2.

The integral cross sections (total, σ_t; momentum transfer, σ_m; viscosity, σ_v and energy-loss, σ_1) are shown in figures 5–7 in the whole energy region considered here. First we discuss our low-energy (below 1 eV) integral and momentum transfer cross sections shown in figures 5(*a*) and 6 (see the inset) respectively. Our value of the cross section near the RT minimum is about 2.8×10^{-16} cm^2 for σ_t and 0.4×10^{-16} cm^2 for σ_m. The swarm data of Kurachi and Nakamura (1989) gives a minimum value of about 1.1×10^{-16} cm^2 in their σ_m curve, while Hayashi (1987) estimates this minimum value to be 0.5×10^{-16} cm^2 . Finally, we can conclude from figures 5(*a*) and

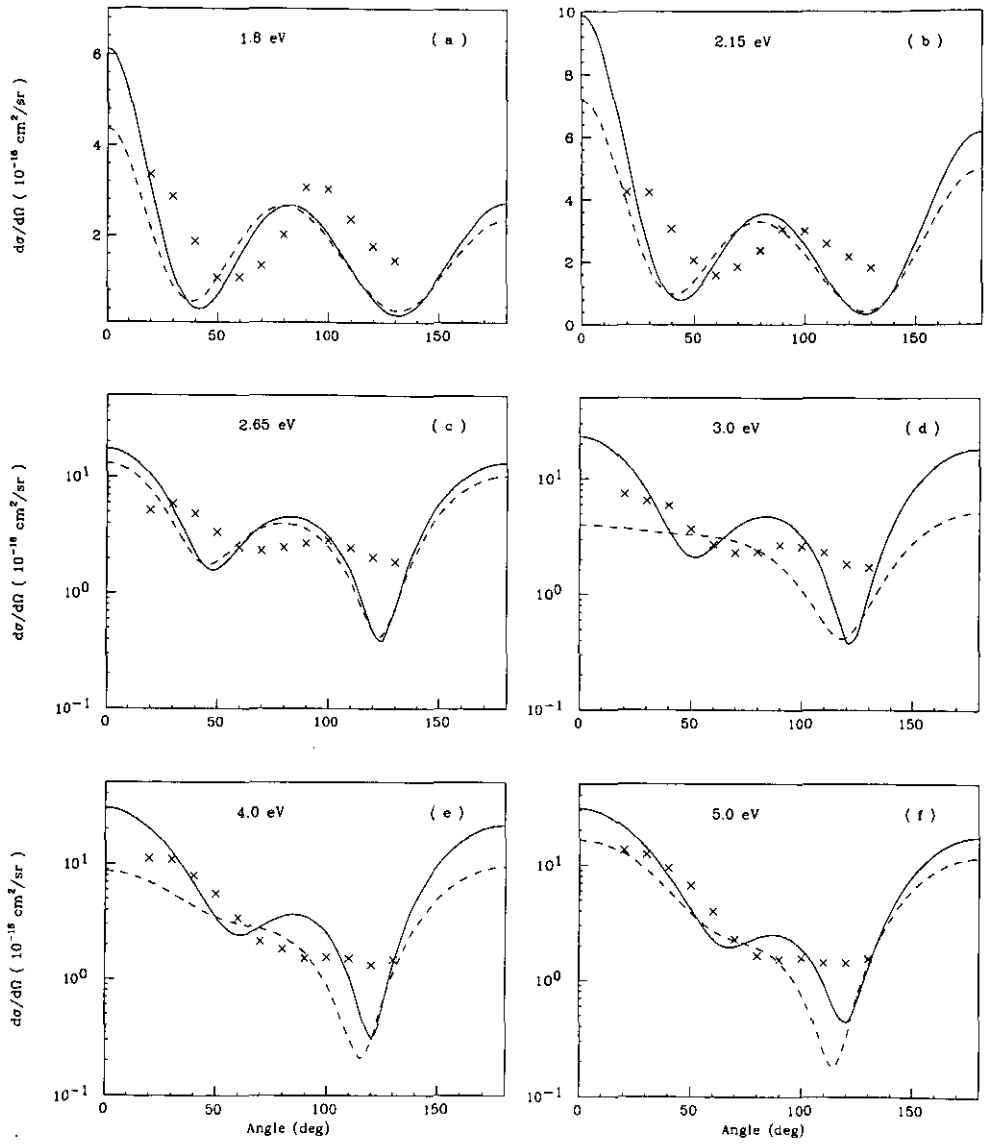

Figure 4. (*a*) Rotationally summed (vibrationally elastic) differential cross sections for the e–SiH_4 collisions at 1.8 eV. Theory: full curve, present ESEP model; broken curve, present ESE model. Experiment: crosses, Tanaka et al (1990). (*b*) as (*a*) but at 2.15 eV. (*c*) as (*a*) but at 2.65 eV. (*d*) as (*a*) except at 3 eV. (*e*) as (*a*) except at 4 eV. (*f*) as (*a*) except at 5 eV. (*g*) as (*a*) but at 7.5 eV. (*h*) as (*a*) except at 10 eV. (*i*) as (*a*) except at 15 eV. (*j*) as (*a*) except at 20 eV.

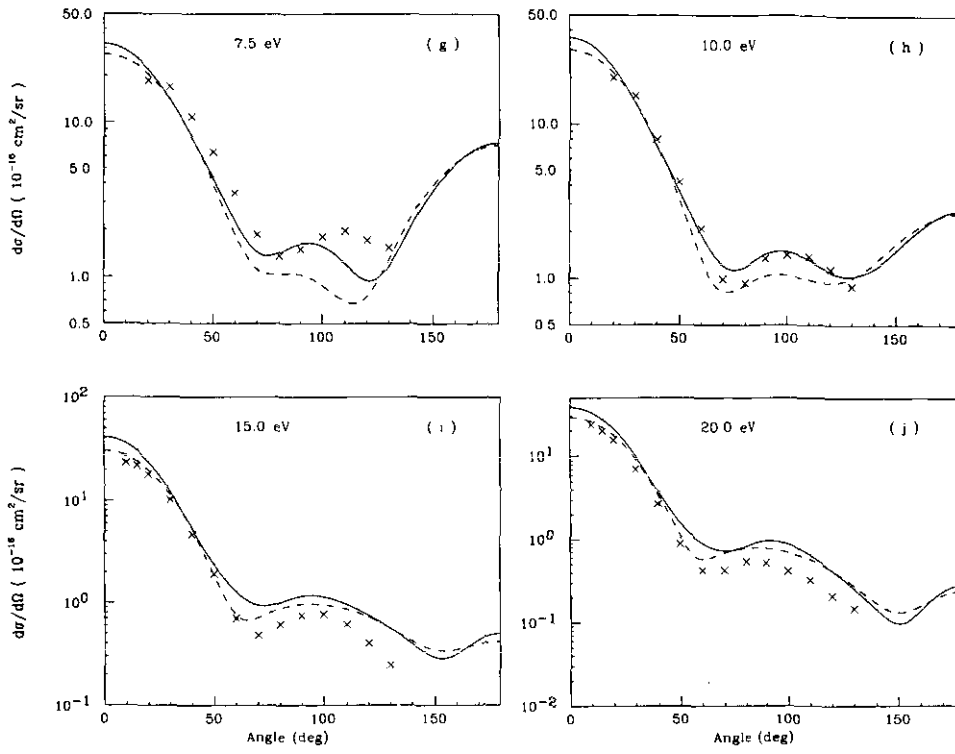

Figure 4. (Continued)

6 that the agreement between present theory (ESEP model) and experimental results is rather encouraging keeping in mind that this low-energy region is quite difficult to study both in theory and experiment.

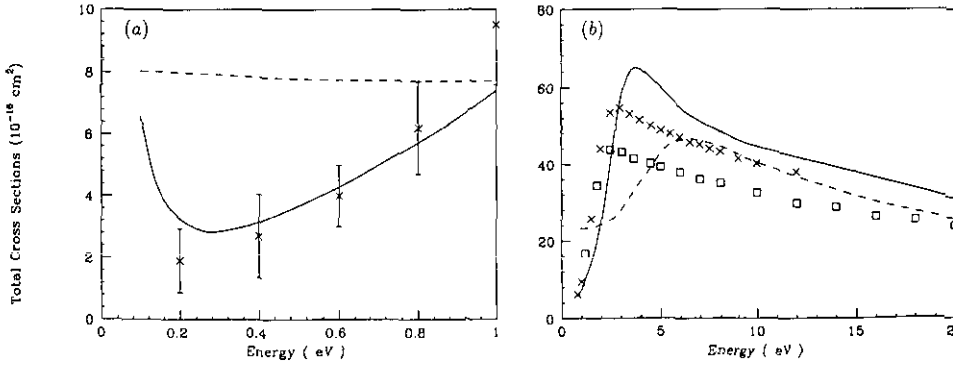

Figure 5. (*a*) Total integral (rotationally summed, vibrationally elastic) cross section for the e–SiH_4 system in the 0.1–1 eV energy range. Full curve, present ESEP; broken curve, present ESE (multiplied by a factor of three). The experimental points (crosses) are taken from Wan *et al* (1989). (*b*) as (*a*) except in the energy range of 1–20 eV. The experimental points are from Wan *et al* (1989) (crosses) and Sueoka and Mori (1985) (squares).

Table 1. Elastic (rotationally summed) cross sections (DCS, σ_t, σ_m and σ_v) for the e–SiH_4 system (10^{-16} cm^2) in the ESEP model from 0.1 to 2.15 eV.

	Energy (eV)							
θ (deg)	0.1	0.2	0.4	0.6	0.8	1.0	1.8	2.15
0	2.67	2.337	2.083	2.009	2.105	2.224	6.121	9.891
5	2.643	2.293	2.025	1.940	2.023	2.133	5.882	9.540
10	2.538	2.167	1.862	1.747	1.793	1.878	5.212	8.551
15	2.382	1.974	1.616	1.460	1.458	1.508	4.236	7.098
20	2.186	1.735	1.323	1.127	1.075	1.088	3.128	5.425
30	1.739	1.215	0.732	0.499	0.394	0.365	1.215	2.409
40	1.314	0.761	0.299	0.117	0.0542	0.0544	0.409	0.895
50	0.972	0.439	0.076	0.0077	0.0566	0.149	0.714	1.012
60	0.720	0.238	0.0049	0.0618	0.232	0.437	1.539	2.005
70	0.536	0.119	0.0124	0.170	0.428	0.722	2.290	3.017
80	0.395	0.0496	0.0544	0.279	0.577	0.916	2.650	3.522
90	0.283	0.0128	0.113	0.372	0.668	0.997	2.544	3.339
100	0.196	0.0005	0.176	0.439	0.694	0.963	2.032	2.547
110	0.132	0.0056	0.231	0.465	0.647	0.818	1.286	1.453
120	0.090	0.0189	0.263	0.443	0.537	0.599	0.594	0.557
130	0.0628	0.0332	0.271	0.385	0.398	0.371	0.264	0.371
140	0.0453	0.0458	0.266	0.318	0.270	0.198	0.462	1.132
150	0.0333	0.0572	0.258	0.263	0.180	0.103	1.096	2.639
160	0.0251	0.0677	0.255	0.228	0.129	0.071	1.880	4.352
170	0.0202	0.0759	0.257	0.211	0.105	0.067	2.497	5.667
180	0.0185	0.0791	0.258	0.206	0.0978	0.069	2.727	6.155
σ_t	6.564	3.246	3.143	4.289	5.717	7.407	19.75	29.25
σ_m	2.823	0.921	2.521	4.169	5.478	6.867	17.56	26.74
σ_v	3.374	1.097	1.330	2.592	4.051	5.657	13.78	18.39

Next we show our σ_t and σ_m values in the 1–20 eV region in figures 5(*b*) and 6 respectively. The experimental data are taken from Sueoka and Mori (1985) and Wan *et al* (1990). There is significant discrepancy between the two sets of measured values. Our present ESEP curve seems to be in fair agreement with the recent measurements of Wan *et al* (1990). The position of the shape resonance in ESEP theory (around 3.75 eV) and experiment (around 3.1 eV) differs by about 20%, while the magnitude of the cross sections in this energy region also has a significant discrepancy; for example, the theoretical (ESEP) peak value of the σ_t is about 20% higher than the measured value of Wan et al (1990). The good agreement above 5 eV between the ESE curve and experimental points (crosses) is definitely fortuitous. Note that the inclusion of polarization effects shifts the shape resonance position from about 6.5 eV to about 3.75 eV and increases its magnitude by about 45%. Thus, the importance of polarization interaction in this energy region cannot be overlooked.

In figure 6, we have plotted our σ_m cross sections at all energies considered here. The swarm points are taken from Kurachi and Nakamura (1989) and Ohmori *et al* (1986). We see a significant discrepancy between theory and experiment; however, there seems to be agreement in the general trend of the cross sections as a function of impact energy. In the resonance energy region, our calculations are much higher than the swarm data. The accuracy of the swarm analysis above 1 eV may be questionable. We also realize that a better polarization potential may be required in the present energy region. Finally, figure 7 illustrates the σ_v values along with energy-loss cross

Table 2. Elastic (rotationally summed) cross sections (DCS, σ_t, σ_m and σ_v) for the e–SiH_4 system (10^{-16} cm^2) in the ESEP model from 2.65 to 20.0 eV.

	Energy (eV)							
θ (deg)	2.65	3.0	4.0	5.0	7.5	10.0	15.0	20.0
0	17.43	22.73	30.01	30.56	32.04	35.81	40.93	38.48
5	16.90	22.09	29.29	29.88	31.27	34.82	39.57	37.08
10	15.37	20.27	27.27	27.96	29.07	32.02	35.76	33.20
15	13.11	17.54	24.20	25.05	25.78	27.88	30.21	27.57
20	10.45	14.29	20.48	21.51	21.89	23.05	23.87	21.23
30	5.37	7.906	12.78	14.10	14.09	13.77	12.35	10.08
40	2.275	3.629	6.795	8.044	8.127	7.284	5.361	3.826
50	1.608	2.146	3.496	4.187	4.367	3.707	2.390	1.578
60	2.498	2.648	2.511	2.365	2.286	1.932	1.316	0.933
70	3.751	3.844	2.878	2.018	1.445	1.233	0.974	0.759
80	4.475	4.646	3.501	2.338	1.428	1.228	1.033	0.857
90	4.242	4.437	3.479	2.453	1.632	1.451	1.186	0.983
100	3.096	3.180	2.498	1.891	1.570	1.504	1.170	0.908
110	1.551	1.480	1.066	0.921	1.225	1.337	0.991	0.680
120	4.724	0.405	0.308	0.413	0.965	1.139	0.783	0.457
130	7.194	1.009	1.367	1.289	1.197	1.079	0.600	0.297
140	2.656	3.731	4.724	3.964	2.107	1.216	0.439	0.192
150	5.885	8.064	9.860	8.075	3.612	1.565	0.346	0.152
160	9.412	12.75	15.40	12.56	5.372	2.087	0.381	0.198
170	12.10	16.32	19.65	16.06	6.826	2.600	0.505	0.297
180	13.09	17.64	21.23	17.37	7.395	2.819	0.574	0.349
σ_t	45.89	56.06	64.87	60.08	50.16	45.17	37.94	30.85
σ_m	42.81	52.03	55.98	46.46	29.15	20.95	12.84	9.04
σ_v	24.67	27.36	26.39	22.75	19.23	17.21	13.07	9.85

sections. The dominance of the 3–4 eV feature is seen in these curves too (figure 7).

3.2. Rotationally elastic and inelastic cross sections

At very low energies, the energy loss of the incoming projectile due to the rotational channel is a very important mechanism in e–molecule collisions. It is now possible to measure indirectly the rotational excitation cross sections for electron–molecule systems (Müller *et al* 1985). With this possibility in mind, we discuss our rotationally elastic and inelastic cross sections. First, we present our rotationally elastic and inelastic differential cross sections in figures 8(*a*), (*b*), (*c*), (*d*), (*e*) and (*f*) at 0.5, 3, 5, 10, 15 and 20 eV respectively. As expected, the elastic $0 \rightarrow 0$ channel dominates all other inelastic processes at all angles except at those angles where a deep minimum occurs in the $0 \rightarrow 0$ DCS. Also shown in these figures are the energy-loss DCS (crosses) summed over all final rotational states. From a qualitative point of view, the general shape of rotationally inelastic DCS for the e–SiH_4 system is quite similar to the corresponding CH_4 curves (see McNaughten *et al* 1990). The $0 \rightarrow 4$ transition depends weakly on the scattering angle, while the $0 \rightarrow 3$ one has considerable angular dependence. The $0 \rightarrow 6$ cross sections are generally smaller; however, as the energy is increased, they become larger than the other transitions at certain scattering angles. The total energy-loss DCS are almost flat with respect to angular variation. It is also clear from these figures that a spherical approximation may not be an appropriate

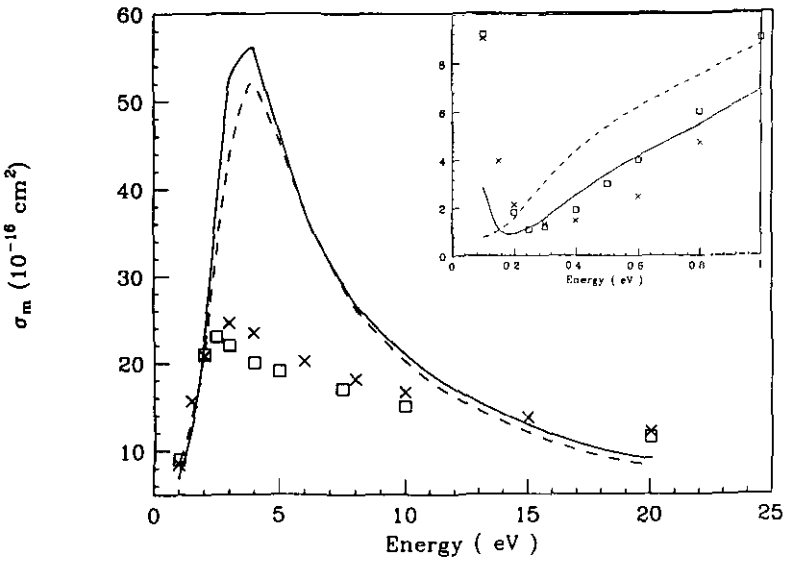

Figure 6. Momentum transfer cross sections for the e–SiH_4 collisions in the present ESEP (full curve) and ESE (broken curve) models. In the inset, we have shown more clearly the results at low (below 1 eV) energies. The experimental points are taken from Kurachi and Nakamura (1989) (squares) and Ohmori et al (1986) (crosses).

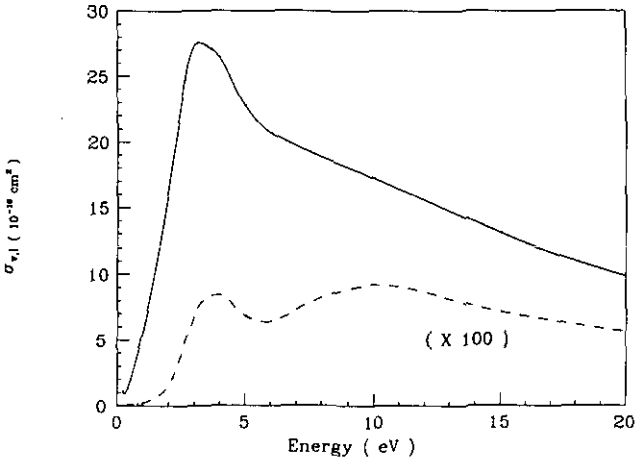

Figure 7. Viscosity, σ_v, (full curve) and energy-loss, σ_l, (broken curve) cross sections for the e–SiH_4 collision in the whole energy (0.2–20 eV) range. Note that the energy-loss numbers are multiplied by a factor of 100.

model for the total DCS in this energy range. We do not have any other data to compare with the results of figures 8(*a*)–(*f*).

It may be interesting to see the effect of the polarization potential on the rotational excitation process. Due to symmetry of the polarization term (only the spherical, $l = 0$, term was included in the calculation) for the T_d point group, the first Born approximation (FBA) will give zero cross section from the polarization potential term

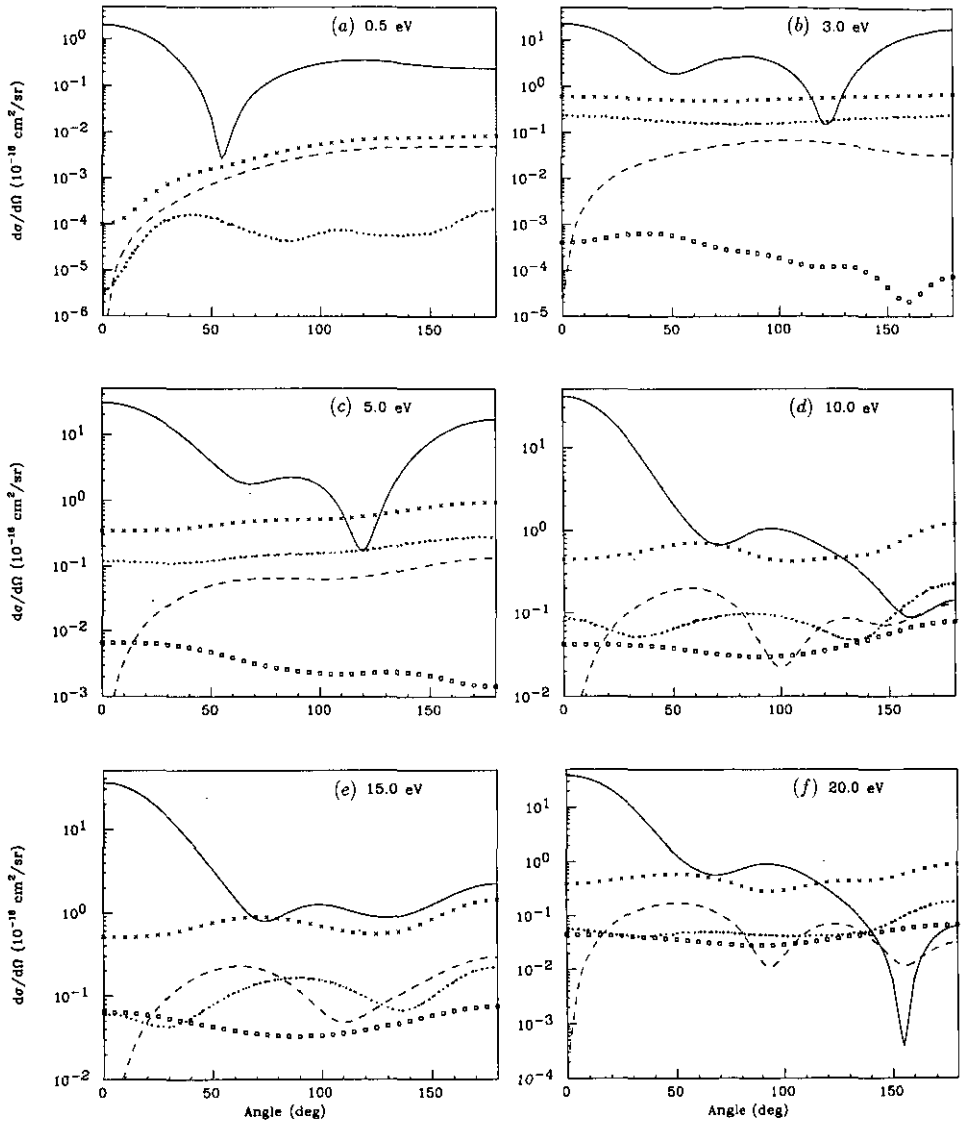

Figure 8. (*a*) Rotationally elastic and inelastic differential cross sections for e–SiH_4 scattering in the ESEP model at 0.5 eV. Full curve, 0 → 0; broken curve, 0 → 3; dotted curve, 0 → 4; squares, 0 → 6; crosses, energy-loss (rotationally summed) differential cross sections. (*b*) as (*a*) except at 3 eV. (*c*) as (*a*) except at 5 eV. (*d*) as (*a*) except at 10 eV. (*e*) as (*a*) except at 15 eV. (*f*) as (*a*) except at 20 eV.

only. In the present calculation, we, however, see a substantial difference in the DCS with and without polarization effects. In figures 9 and 10, we have shown a comparison of ESE and ESEP DCS for all three transitions ($0 \rightarrow 3$, $0 \rightarrow 4$ and $0 \rightarrow 6$) at 5 eV and 10 eV respectively. In general, the ESEP cross sections are higher than the corresponding ESE values and, in addition, exhibit more features. These figures (9 and 10) demonstrate that a polarized target is more efficient at exciting its rotational modes through the angular momentum transfer from the projectile. We will see later the same comparison for integral cross sections at all energies considered here.

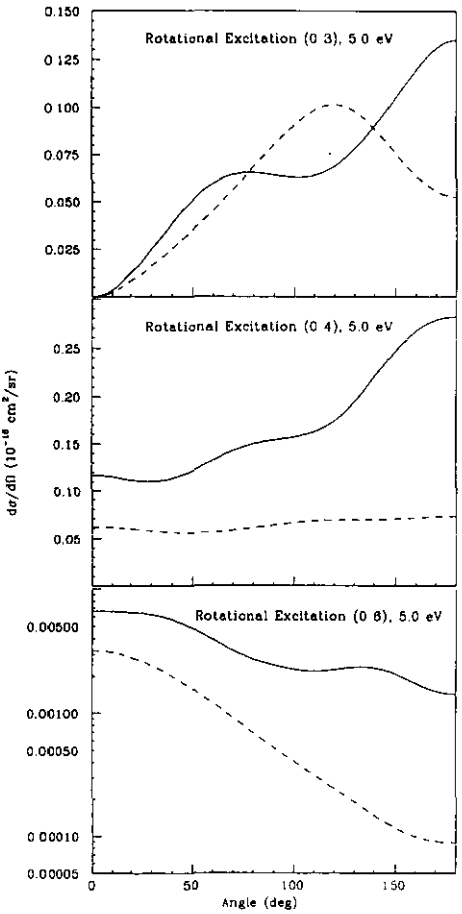

Figure 9. Differential cross sections for rotationally inelastic transitions with (full curves, ESEP model) and without (broken curves, ESE model) polarization effect at 5 eV.

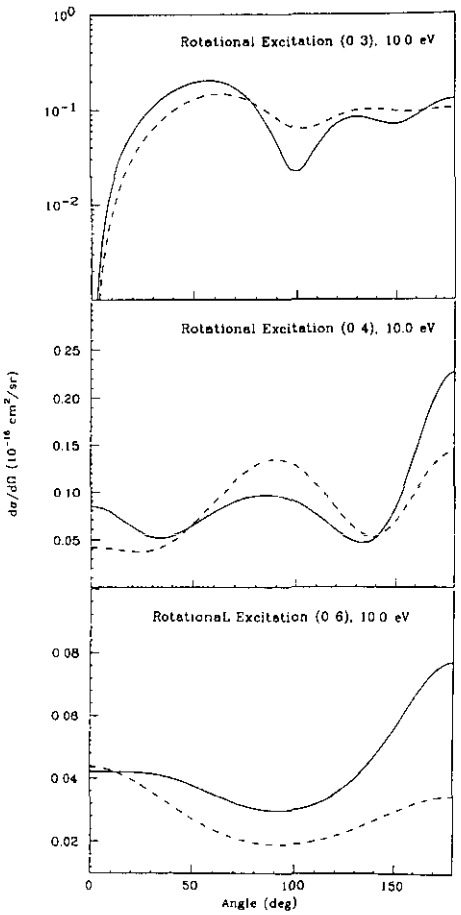

Figure 10. As in figure 9 except at 10 eV.

We now discuss the integral values of various rotational excitation cross sections. In figures 11–14, we have shown our integral (full curves) and momentum transfer (broken curves) values for all the four cases, i.e. $\sigma^{00}_{t,m}$, $\sigma^{03}_{t,m}$, $\sigma^{04}_{t,m}$ and $\sigma^{06}_{t,m}$. As expected, the pure elastic process has all the main features (RT minimum and the 3–4 eV shape resonance) of the total scattering process. The rotational channels are small, but

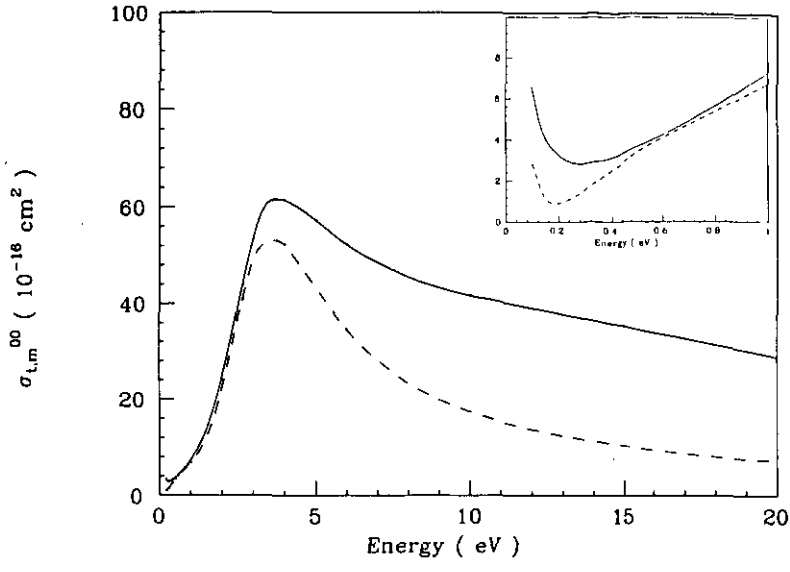

Figure 11. σ_t^{00} (full curve) and σ_m^{00} (broken curve) cross sections for e–SiH_4 collisions in the ESEP model. In the inset, we show more clearly the low-energy (below 1 eV) data.

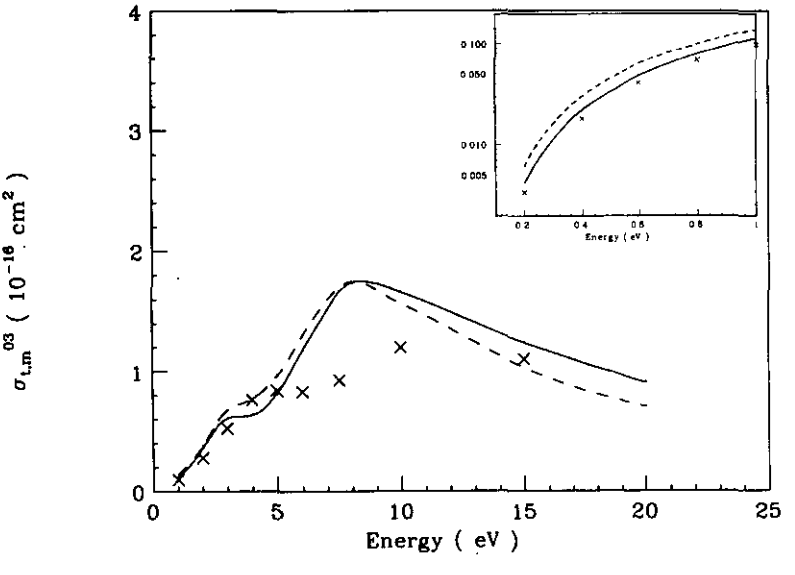

Figure 12. As figure 11 except for the inelastic 0 → 3 transition. The crosses are the σ_t^{03} values in the ESE model. In the inset, we show the same data below 1 eV energy.

exhibit interesting features in the energy distribution of their cross sections. For example, the 0 → 3 curves in figure 12 have enhancement in the cross sections around 8 eV, while the 3–4 eV region shows a weak structure (remember there is a 3–4 eV shape resonance here in the elastic and total cross sections). The 0 → 4 cross sections

are, however, enhanced in the 3–4 eV region. It is interesting to notice that this structure is produced mainly due to the polarization effect (see the crosses in figure 13, which represent the ESE σ_t^{04} values). Finally, the $0 \rightarrow 6$ cross sections (figure 14) are also characterized by an enhancement around 10 eV. Here, also, we see a significant change in the inelastic cross sections when polarization effects are included (see the crosses in figure 14). In the inset to figure 14, we have shown low-energy (below 1 eV) $\sigma_{t,m}^{06}$ results with and without polarization effects. Some strange features in the ESEP curves around 1 eV are seen for which we have no explanation at this time.

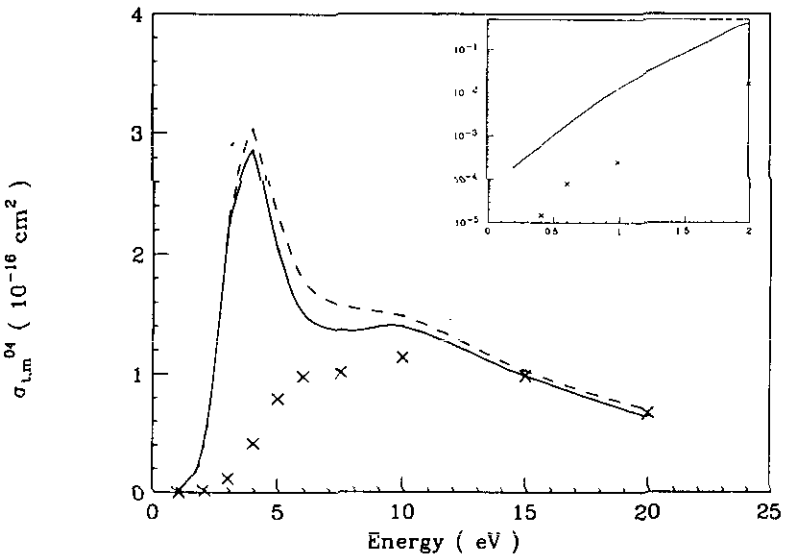

Figure 13. As in figures 11 and 12 except for the $0 \rightarrow 4$ rotational excitation.

Finally, we want to show our integrated energy-loss cross sections in all the three ($\Delta J = 3, 4, 6$) transitions computed, with and without polarization effects. Figure 15 depicts the ESEP σ_l^{03} (full curve), σ_l^{04} (broken curve) and σ_l^{06} (dotted curve) values, while figure 16 shows the same cross sections in the ESE model. We see clearly that the inclusion of polarization effects changes the behaviour of the energy-loss cross sections with respect to the projectile energy. At higher energies ($E \geq 15$ eV), the $0 \rightarrow 6$ transition dominates over other lower-order rotational excitations. The $0 \rightarrow 4$ cross sections are always higher than the $0 \rightarrow 3$ ones except at lower energies (below 2 eV), where the $0 \rightarrow 3$ transition dominates over all higher excitations. The total energy-loss or the stopping cross sections, shown earlier in figure 7, are independent of the initial J value of the rotational state of the target. This agrees with a general theorem due to Shimamura (1981, 1983) that the stopping cross sections, when summed over all final rotational states, are independent of the initial rotational state of the molecule in a situation where the adiabatic-nuclei-rotation approximation is valid. We have checked the σ_l values with several initial J values and found that the above theorem is correct.

We have extended our calculations further at lower energies towards the zero-energy limit. For example, at 0.001, 0.0025, 0.005, 0.01, 0.025 and 0.05 eV energies the values of the σ_t (σ_m) are (in units of 10^{-16} cm^2) 47.82 (46.45), 42.53 (40.4), 37.42

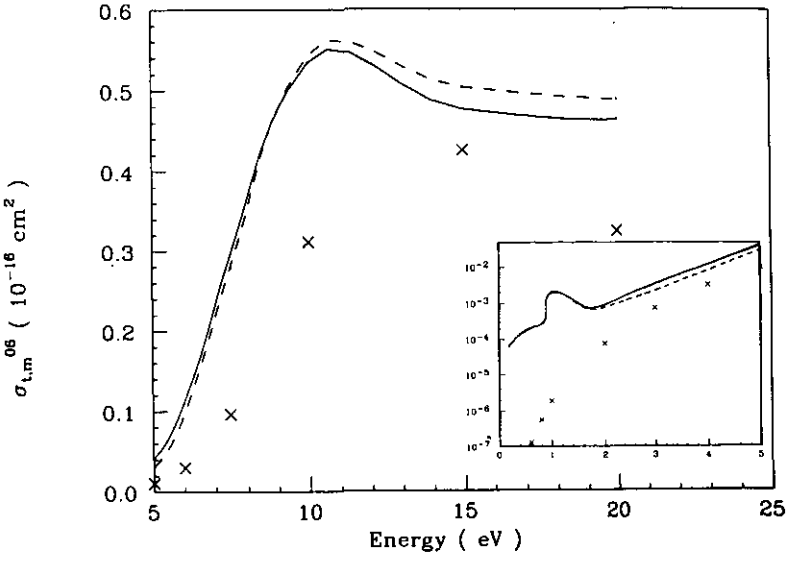

Figure 14. As in figures 11 and 12 except for the $0 \rightarrow 6$ transition.

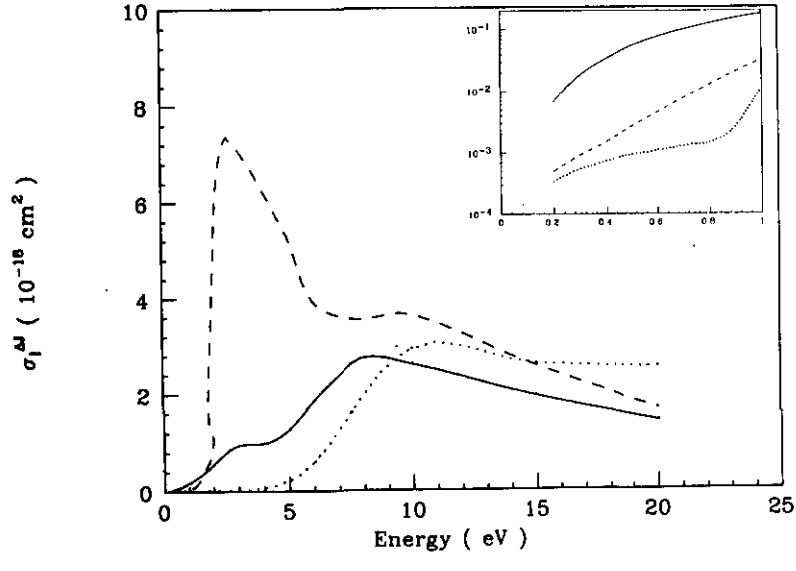

Figure 15. Energy-loss (integral) cross sections for various rotational transitions for e–SiH_4 scattering in the ESEP model as a function of impact energy. Full curves, $0 \rightarrow 3$; broken curves, $0 \rightarrow 4$; dotted curves, $0 \rightarrow 6$.

(34.64), 30.88 (27.63), 20.68 (16.63) and 12.83 (8.58) respectively. At 0.01 eV, the σ_m values given by various swarm studies are 56.0 (Hayashi 1987), 66.0 (Ohmori *et al* 1986) and 32.0 (Kurachi and Nakamura 1989). It is rather frustating to see such a large discrepancy between these swarm values for the σ_m value at this low energy. It may be interesting to use our ESEP σ_m values in the swarm analysis. The value of scattering length is estimated to be −4.2 au in our present ESEP calculation.

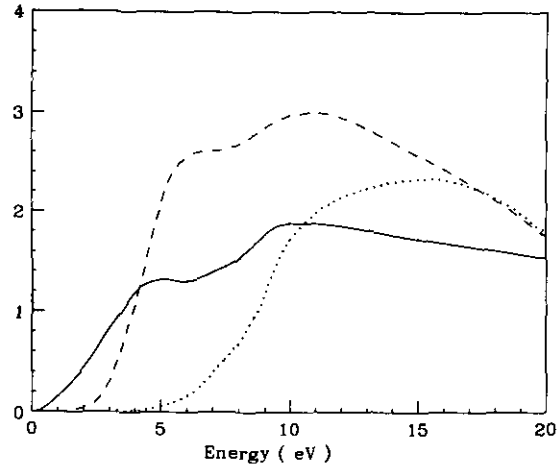

Figure 16. As figure 15 except in the ESE model (without any polarization effect).

4. Conclusions

We have presented differential, integral, momentum transfer, viscosity and stopping power cross sections for the e–SiH_4 rotationally elastic, inelastic and summed processes from very low energy (0.001 eV) to up to 20 eV. The exchange interaction is included exactly while polarization (and correlation) effects are considered approximately via a parameter-free (with non-adiabatic correction) model potential. We have compared these results with available measurements and the agreement is encouraging. Our calculation confirms the d-wave component in the T_2 representation responsible for the 3–4 eV shape resonance phenomenon. This feature is also contributed by the E symmetry. The lifetime of this shape resonance is less than 10^{-15} s. The scattering length is found to be about -4.2 au, which is larger than the CH_4 scattering length. Our main conclusions are the following: (i) the polarization effects are essential in this energy region, for all the collision processes (rotationally elastic, inelastic and summed) considered here; (ii) there is a significant discrepancy between the two sets of available experimental data on the total cross sections; there is, therefore, a need for more experimental studies on the σ_t values; (iii) further measurements on the absolute differential cross sections are also required in order to see the usefulness of the present theory. Compared with the e–CH_4 system, the experimental as well as theoretical situation on the e–SiH_4 collision is not satisfactory.

Acknowledgments

This research is funded by the US Department of Airforce, Wright-Patterson Air Force Base, under the contract no FY33615-90-C-2032. The computational facilities were provided by the FSU Supercomputer Research Institute (SCRI). One of us (AJ) thanks the SCRI staff for their continous support. We thank Professor Franco Gianturco for fruitful discussions.

References

Birnbaum G and Cohen E R 1976 *Mol. Phys.* **32** 161

Chase D M 1956 *Phys. Rev.* **104** 838

Garscadden A, Duke G L and Bailey W F 1983 *Appl. Phys. Lett.* **43** 1012

Gianturco F A and Jain A 1986 *Phys. Rep.* **143** 348

Gianturco F A, Pantano L C and Scialla S 1987 *Phys. Rev.* A **36** 557

Giordan J C 1983 *J. Am. Chem. Soc.* **105** 6544

Hara S 1967 *J. Phys. Soc. Japan* **22** 710

Hayashi M 1987 *Swarm Studies and Inelastic Electron–Molecule Collisions* ed L C Pitchford *et al* (Berlin: Springer) pp 167

Hill N E, Vaugham W E, Price W E and Davies M 1969 *Dielectronic Properties and Molecular Behavior* (New York: Van Nostrand)

Jain A 1983 *PhD Thesis* Queen's University, Belfast

—— 1987 *J. Chem. Phys.* **86** 1289

Jain A and Thompson D G 1982 *J. Phys. B: At. Mol. Phys.* **15** L631

—— 1983 *J. Phys. B: At. Mol. Phys.* **16** 3077

—— 1987 *J. Phys. B: At. Mol. Phys.* **20** 2861

Jain A K, Tripathi A N and Jain A 1987 *J. Phys. B: At. Mol. Phys.* **20** L389

Jain A, Weatherford C A McNaughten P and Thompson D G 1989 *Phys. Rev.* A **40** 6730

Kurachi M and Nakamura Y 1989 *J. Phys. D: Appl. Phys.* **22** 107

Mathieson K J, Millican P G, Walker I C and Curtis M G 1987 *J. Chem. Soc. Faraday Trans. II* **83** 1041

McNaughten P and Thompson D G 1988 *J. Phys. B: At. Mol. Opt. Phys.* **21** L703

McNaughten P, Thompson D G and Jain A 1990 *J. Phys. B: At. Mol. Opt. Phys.* **23** 2405

Müller R, Jung K, Kochem K H, Sohn W and Ehrhardt H 1985 *J. Phys. B: At. Mol. Phys.* **18** 3971

Norcross D W 1982 *Phys. Rev.* A **25** 764

Ohmori Y, Shimozuma M and Tagashira H 1986 *J. Phys. D: Appl. Phys.* **19** 1029

Pollock W J 1968 *Trans. Faraday Soc.* **64** 2919

Pople J A and Schofield P 1957 *Phil. Mag.* **2** 591

Salvini S S and Thompson D G 1981 *J. Phys. B: At. Mol. Phys.* **14** 3797

Shimamura I 1981 *Phys. Rev.* A **23** 3350

—— 1983 *Phys. Rev.* A **28** 1357

Sueoka O and Mori S 1985 *At. Coll. Res. Japan* **11** 19

Tanaka H, Boesten L, Sato H, Kimura M, Dillon M A and Spence D 1990 *J. Phys. B: At. Mol. Opt. Phys.* **23** 577

Temkin A 1957 *Phys. Rev.* **107** 1004

Tossell J A and Davenport J W 1984 *J. Chem. Phys.* **80** 813

Tronc M, Hitchcock A and Edard F 1989 *J. Phys. B: At. Mol. Opt. Phys.* **22** L207

Wan Hai-Xing, Moore J H and Tossell J A 1989 *J. Chem. Phys.* **91** 7340

Winstead C, Hipes P G, Pritchard H P and Mckoy V 1990 *Bull. Am. Phys. Soc.* **35** 1141

Yuan J 1989 *J. Phys. B: At. Mol. Opt. Phys.* **22** 2589